RSC Advances

ROYAL SOCIETY OF CHEMISTRY

www.rsc.org/advances

Heterojunctions Generated in SnO_2-CuO Nanocatalysts for Improved Catalytic Property in Rochow Reaction

Shanying Zou,[a,b] Yongjun Ji,[b,*] Guangna Wang,[b] Yongxia Zhu,[b]

Hezhi Liu,[b] Lihua Jia,[a] Xiangfeng Guo,[a,*] Ziyi Zhong[c] and Fabing Su[b,*]

[a] *College of Chemistry and Chemical Engineering, Qiqihaer University, Qiqihaer 161006, Heilongjiang Province, China.*

[b] *State Key Laboratory of Multiphase Complex Systems, Institute of Process Engineering, Chinese Academy of Sciences, Beijing 100190, China.*

[c] *School of Chemical & Biomedical Engineering, Nanyang Technological University, 62 Nanyang Drive, Singapore 637459.*

*To whom correspondence should be addressed. E-mail address: yjji@ipe.ac.cn (Y. Ji), xfguo@163.com (X. Guo), fbsu@ipe.ac.cn (F. Su), Tel.: +86-10-82544850, Fax: +86-10-82544851.

Abstract

We report the improved catalytic performance of SnO_2-CuO hybrid nanocatalysts synthesized by rationally designing and controlling the local heterojunctions structure. The SnO_2 nanoparticles (NPs) decorated CuO nanorods (NRs) (SnO_2-CuO) with a mace-like structure and with various CuO : SnO_2 ratios were prepared via depositing pre-synthesized SnO_2 NPs on CuO NRs in the presence of polyvinylpyrrolidone molecules. The CuO NRs were obtained by a facile hydrothermal reaction using $Cu(NO_3)_2$•$3H_2O$ as the precursor. The samples were characterized by X-ray diffraction, transmission electron microscopy, scanning electron microscopy, X-ray photoelectron spectroscopy, and temperature-programmed reduction analyses. The results indicated that in the SnO_2-CuO hybrid nanostructures, the heterojunctions were well generated as the SnO_2 NPs were well dispersed on the CuO NRs. Their catalytic performances were then explored via the Rochow reaction, in which solid silicon (Si) reacts with gaseous methyl chloride (MeCl) to produce dimethyldichlorosilane (M2). Compared to discrete CuO and SnO_2 as well as their physical mixture, the SnO_2-CuO hybrids exhibit significantly enhanced M2 selectivity and Si conversion because of the enhanced synergistic interaction between SnO_2 and CuO due to the generated heterojunctions. This work demonstrates that the performance of heterogeneous catalysts can be improved by carefully designing and controlling its structures even maintaining the composition unchanged.

Keywords: CuO nanorods; SnO_2 nanoparticles; heterojunctions; catalytic property; Rochow reaction.

1. Introduction

Because of the obvious growth of the silicone industry in the past few decades, there has been evidenced a stable increase in the production of methylchlorosilanes (MCSs), which serve as the primary monomeric intermediates for the manufacture of silicone products via the Rochow reaction.[1,2] In this reaction, gaseous methyl chloride (MeCl) reacts with silicon (Si) in the presence of Cu-based catalysts as following:[3-5]

$$\mathrm{Si + MeCl} \xrightarrow[300\text{-}350^{o}\mathrm{C}]{\text{copper catalyst}} \begin{cases} (CH_3)_3SiCl \\ (CH_3)_2SiCl_2 \\ CH_3SiCl_3 \\ CH_3HSiCl_2 \\ (CH_3)_2HSiCl \\ \text{other low boilers} \\ \text{residue} \end{cases} \quad (1)$$

Among these products, dimethyldichlorosilane ($(CH_3)_2SiCl_2$, M2) is the most important monomer for the production of organosilane products in industry.[6] Therefore, a high M2 yield is always demanded. As reported, the catalysts used in the Rochow reaction are various Cu-based catalysts, including metallic Cu powders,[7] CuCl,[8,9] Cu_2O,[10] Cu,[11] Cu-Si alloy,[12] and Cu-Cu_2O-CuO,[13] and the promoters include Sn-based additives.[5,14] In the past few years, porous cubic structures such as Cu microparticles,[15] mesoporous Cu_2O microspheres,[10] flower-like,[16] and hierarchical dandelion-like CuO microspheres[17] have been prepared in our group as model catalysts for the Rochow reaction, and found that their catalytic performance mainly depends on the chemical composition,[18] particles size,[19] and surface structure.[16] However, the above catalysts still suffer from low M2 selectivity and/or Si conversion, which seriously hinder their further application. Therefore, more efficient Cu-based catalysts should be developed.

Recently, CuO-based hetero-structured hybrid materials have caused strong attention owing to their distinct properties and high diversity in structure and composition. For instance,

Avgouropoulos *et al.* prepared a series of CuO-CeO_2 catalysts which exhibited much better catalytic performance for the selective oxidation of CO than CuO alone.[20] Li *et al.* observed that the CuO-ZnO-ZrO_2 catalysts synthesized by a surfactant-assisted coprecipitation method showed higher catalytic activity than that of sole CuO as a result of more intimate contact at the interface between Cu species and ZnO and/or ZrO_2.[21] More recently, we have grown flower-like ZnO on urchin-like CuO microspheres using a simple solvothermal method, and the hierarchical structure displayed better catalytic properties in M2 synthesis in comparison with the single CuO phase, probably because of the enhanced synergistic effect between ZnO and CuO.[22] However, the composite particles were still in the micrometer scale with limited particle contact and weak synergistic effect. On the other hand, to date there are few reports on preparing Cu-based nanocatalysts for Rochow reaction, which may show superior catalytic properties to their bulk counterparts. In addition, lowering the particle size to nanoscale may create more intimate contacts at the interfaces which will offer more possibilities to tune the catalytic property. This motivated us to design Cu-based nanoscale heterostructures for Rochow reaction. Furthermore, considering that SnO_2 is an effective promoter in Rochow reaction, we prepared CuO nanorods (NRs) and then rationally loaded pre-made SnO_2 nanoparticles (NPs) on them to construct a novel mace-like hybrid as the model catalyst. Compared with single CuO and SnO_2 phases as well as their physical mixture, the SnO_2-CuO mace-like hybrid nanocatalysts did show much higher M2 selectivity and Si conversion, obviously originated from the enhanced synergistic effect between CuO and SnO_2. Also, the relationship between the enhanced catalytic performance and the structure is studied.

2. Experimental

2.1. Material synthesis

Copper nitrate trihydrate ($Cu(NO_3)_2•3H_2O$, A.R., 99.0%), ethanol (CH_3CH_2OH, A.R., 99.0%), ammonia solution (NH_4OH, A.R., 25.0-28.0%), sodium hydroxide (NaOH, A.R., 99.0%), acetone (CH_3COCH_3, A.R., 99.5%) were purchased from Xilong Chemical Reagent Co. Ltd., China. Stannic chloride pentahydrate ($SnCl_4•5H_2O$, A.R., 99.0%) and polyvinylpyrrolidone (PVP, MW 40 000) were obtained from Sinopharm Chemical Reagent Co. Ltd., Shanghai, China. All chemicals were used as received without further purification.

The CuO NRs were prepared by a facile hydrothermal method. In a typical synthesis, 0.1 g of $Cu(NO_3)_2•3H_2O$ and 0.003 g of PVP were dissolved into 3.0 mL of ethanol to form a homogeneous solution, followed with addition of 10.0 mL of NaOH aqeous solution (5.0 M). The obtained gel was transferred into a 100 mL of Teflon-lined stainless-steel autoclave, which was sealed and maintained at 140 ^oC for 24 h before it was cooled down to room temperature. Finally, the resulting solid precipitate was collected by filtration, washed with deionized water and ethanol for several times, and dried at 60 ^oC for 8 h. On the other hand, the SnO_2 NPs were synthesized by modifying the previously reported procedures,[23] using $SnCl_4•5H_2O$ as the precursor and NH_4OH as the precipitating agent. Briefly, 8.8 g of $SnCl_4•5H_2O$ was dissolved in 250.0 mL of deionized water to get a clear solution with a Sn ion concentration of 0.1 M， and then NH_4OH solution was added dropwise under vigorous magnetic stirring until the PH value reached ～7. After maintained for 1 h, the precipitate was filtered, washed with deionized water and acetone for three times, and dried at 80 °C for 6 h. It was further calcined in air at 600 °C for 3 h to obtain the SnO_2 NPs.

SnO_2-CuO hybrid mace-like nanocatalysts were synthesized by adding a desirable amount of pre-made SnO_2 NPs into a CuO NRs suspension in ethanol in the presence of PVP as shown in Fig. 1. Typically, 0.1 g of CuO NRs were firstly dispersed in 100.0 mL of ethanol, followed with addition of the desired amounts of SnO_2 and 0.005 g of PVP under continuous stirring. After

mechanically stirred for 12 h at room temperature, the product was collected by filtration and ethanol wash, and further dried at 60 ^{o}C for 8 h. The synthesis was carried out by fixing the CuO amount at 0.1 g while varying the amount of added SnO_2. The prepared samples are thus denoted as 0.1 wt.% SnO_2-CuO, 0.2 wt.% SnO_2-CuO, 0.5 wt.% SnO_2-CuO, 1.0 wt.% SnO_2-CuO, 5.0 wt.% SnO_2-CuO and 10.0 wt.% SnO_2-CuO according to their measured compositions when the amount of SnO_2 was 0.1, 0.2, 0.5, 1, 5 and 10 mg, respectively. For control experiment, a physical mixture of SnO_2 NPs and CuO NRs was prepared by mixing two samples at a mass ratio of 1:100. The sample is denoted as 1.0 wt.% SnO_2+CuO.

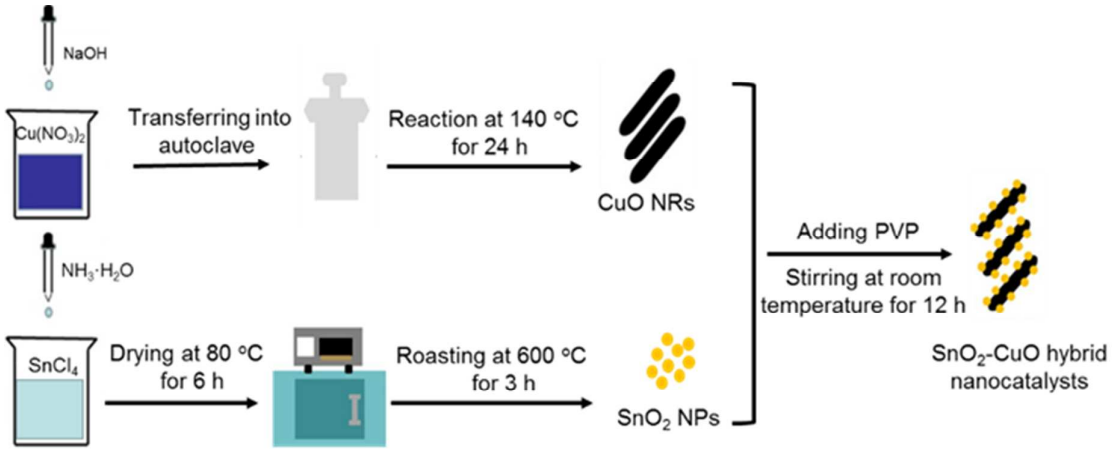

Fig. 1 Preparation process of the SnO_2-CuO hybrid nanocatalysts.

2.2. Characterization

XRD analysis was performed on a PANalytica X'Pert PRO MPD using the Cu Kα radiation (λ=1.5418 Å) at 40 kV and 40 mA. The size of the sample was calculated using the Debye-Scherrer equation. The microscopic features of the samples were observed with field emission scanning electron microscopy (SEM) with energy dispersive spectroscopy (EDS) (JSM-6700F, JEOL, Tokyo, Japan) and transmission electron microscopy (TEM) (JEM-2010F, JEOL, Tokyo, Japan). The HAADF-STEM images were obtained by using 200 kV STEM (JEM-ARM200F, JEOL, Tokyo,

Japan). N_2 adsorption at -196 ^oC was measured using a Quantachrome surface area and pore size analyzer NOVA 3200e. Prior to the measurement, the sample was degassed at 300 ^oC for 3 h under vacuum. The specific surface area was determined according to the Brunauer-Emmett-Teller (BET) method in the relative pressure range of 0.05-0.3. H_2 temperature-programmed reduction (H_2-TPR) was carried out on a Quantachrome automated chemisorption analyzer (ChemBET pulsar TPR/TPD). Briefly, 0.2 g of sample was loaded in a quartz U-tube and heated from room temperature to 200 °C at 10 °C min^{-1} and maintained for 1 h in Ar flow. Then, the sample was cooled to room temperature and followed by heating to 800 °C at 10 °C min^{-1} under a binary gas (10 vol % H_2/Ar in TPR) with a gas flow of 30 mL min^{-1}. X-ray photoelectron spectroscopy (XPS) were taken on ESCALAB 250 (VG) using Al-Kα X-ray source (hv = 1486.6 eV) radiation. The elemental analysis was carried out with Inductively Coupled Plasma Optical Emission Spectrometer (ICP-OES) (Optima 5300DV, perkin Elmer, American).

2.3 Catalytic Measurement

The evaluation of catalytic performance was carried out with a typical MCS lab fixed-bed reactor.[11] 10.0 g of Si powder (20-50 mesh, provided by Jiangsu Hongda New Material Co., Ltd.) was homogeneously mixed with 0.5 g obtained sample and 0.05 g of Zinc (Zn, A.R., Sinopharm Chemical Reagent Co., Ltd.) as a promoter to form a contact mass, which was loaded in the glass reactor. The reactor system was initially preheated for 1 h by heating to 310 ^oC under N_2 gas flow (30 mL min^{-1}). Subsequently, N_2 gas was turned off and MeCl gas with a flow rate of 25 mL min^{-1} was introduced into the reactor to react with Si at 295 ^oC. After a given period of 24 h, the reaction was terminated. The gas product was cooled down into liquid phase with a water circulating bath controlled at -5 ^oC by a programmable thermal circulator (GDH series, Ningbo xinzhi biological

technology Co., LTD). The waste contact mass (residual solid after reaction) containing unreacted Si powder, Cu compounds, and promoters was weighed to calculate Si conversion, while the collected liquid was quantitatively analyzed on a gas chromatograph (GC) (Agilent Technologies 7890A, Thermal conductivity detector, KB-201 column). The products were identified by gas chromatography mass spectrometry (GC-MS) (QP2010, SHIMADZU), which were mainly comprised of methyltricholorsilane (CH_3SiCl_3, M1), M2, trimethylchlorosilane ($(CH_3)_3SiCl$, M3), methyldichlorosilane (CH_3SiHCl_2, M1H), dimethylchlorosilane ($(CH_3)_2SiHCl$, M2H), low boiler (LB) and high boiler (HB). The selectivity of the products was calculated by the peak area ratio (in percentage). The Si conversion (C_{Si}) was calculated according to the following formula:

$$\text{Conversion of Si } (C_{Si}) = \frac{\text{weight}_{\text{contact mass before reaction}} - \text{weight}_{\text{contact mass after reaction}}}{\text{weight}_{\text{Si before reaction}}} \times 100\% \quad (2)$$

3. Results and discussion

3.1. Characterization of synthesized materials

The SEM images in Fig. 2 show the morphology and size of the obtained products. As indicated in Fig. 2a and Fig. S1 in Supporting Information, the as-prepared SnO_2 NPs are nearly spherical with a size range of 20-40 nm. Fig. 2b shows that the as-obtained CuO appears in the form of rods with a length of approximately 0.7-1 μm and a diameter of 20-40 nm, and the surface looks quite smooth and distinct. After the addition of a small amount of SnO_2 NPs into the CuO NRs suspension of ethanol in the presence of PVP and after stirring at room temperature for 12 h, both the morphology and the crystal size of CuO NRs are intact, but the surface becomes rougher due to coating of SnO_2 NPs on the surface of the CuO NRs, suggesting the successful synthesis of SnO_2-CuO hybrids (Fig. 2c). By simply varying the amount of SnO_2 NPs, a series of SnO_2-CuO hybrids can be prepared using this method. Upon further increasing the amount of SnO_2 NPs, more

dense SnO_2 NPs are loaded on CuO hybrids but still maintain the mace-like shape (Fig. 2d and Fig. S2 in Supporting Information). The elemental mapping images (Fig. 2e-h) show the elemental distribution in 1.0 wt.% SnO_2-CuO over large areas, confirming the presence of Cu, O and Sn and their homegeneous distribution. The EDS analysis and line-scanning results further verify the presence of Cu, Sn and O elements (Fig. 2i and Fig. S3 in Supporting Information). Moreover, the Sn : Cu atomic ratios determined by ICP-AES confirm that the compositions of the final products are close to the initial feeding ratio of the components. The specific surface area of SnO_2-CuO hybids, measured from N_2 adsorption isotherms at 77 K, are decreased obviously compared to CuO and SnO_2, as shown in Table 1.

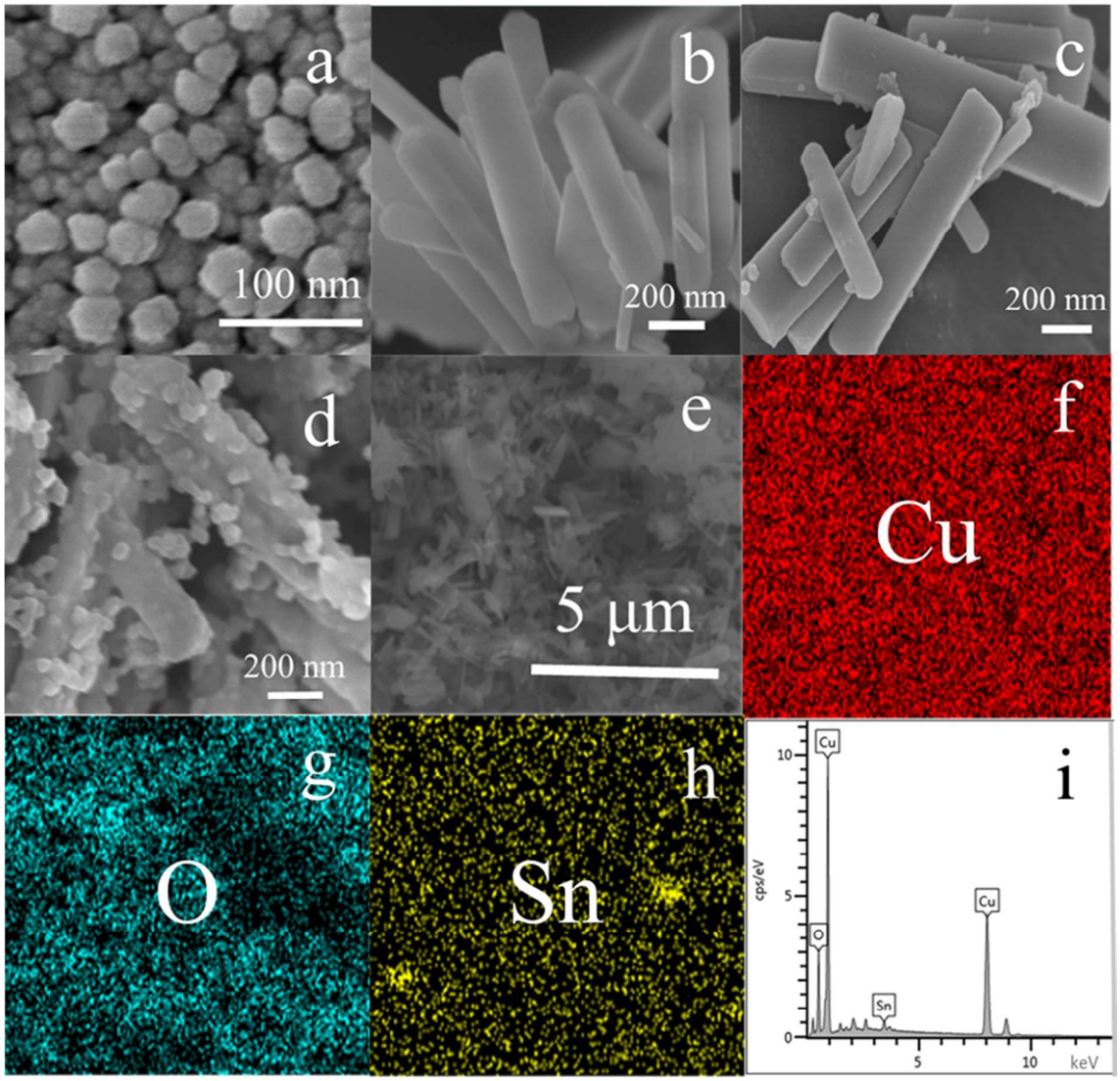

Fig. 2 SEM images of SnO_2 NPs (a), CuO NRs (b), 1.0 wt.% SnO_2-CuO (c), 5.0 wt.% SnO_2-CuO (d), 1.0 wt.% SnO_2-CuO (e), elemental mapping images of Cu (f), O (g), Sn (h) of 1.0 wt.% SnO_2-CuO, and corresponding EDS spectrum (i).

Fig. 3a shows the XRD patterns of CuO NRs, SnO_2 NPs, and the SnO_2-CuO hybrids with various ratios. All samples have high diffraction intensity, indicating their good crystallinity. In the case of pure CuO NRs (Fig. 3a), the observed diffraction peaks are located at 2θ values of 32.5°, 35.6°, 38.7°, 48.8°, 53.4°, 58.2°, 61.6°, 66.3°, 68.0°, 72.3° and 75.0°, corresponding respectively to the lattice planes of (110), (-111), (111), (-202), (020), (202), (-113), (-311), (220), (311) and (004)

of monoclinic CuO (JCPDS No. 03-065-2309). For pure SnO_2 NRs, the diffraction peaks at 2θ values of 26.2°, 33.9° and 51.8° can be indexed to the lattice planes of (110), (101) and (211) of tetragonal SnO_2 (JCPDS No. 01-077-0452). However, in addition to the above CuO diffraction peaks, no peaks of SnO_2 can be traced for 1.0 wt.% SnO_2-CuO due to the very small ratio of SnO_2 in the hybrid that goes beyond the detection limit. With the increase of SnO_2 content, the diffraction peak of tetragonal SnO_2 becomes visible and progressively increased in intensity (5.0 wt.% SnO_2-CuO hybrid to 10.0 wt.% SnO_2-CuO hybrid), as observed clearly by an enlarged view of the XRD patterns in the 2θ range of 24-30° (Fig. 3b). The grain size of CuO and SnO_2 in each sample was calculated by using the Scherer formula based on the 2θ values of 35.5° and 26.6°, respectively, and these data are compiled in Table 1. It can be seen that the grain size of the CuO and SnO_2 in the SnO_2-CuO hybrids are in the same range as those of pure CuO, SnO_2, and their mechanical mixture.

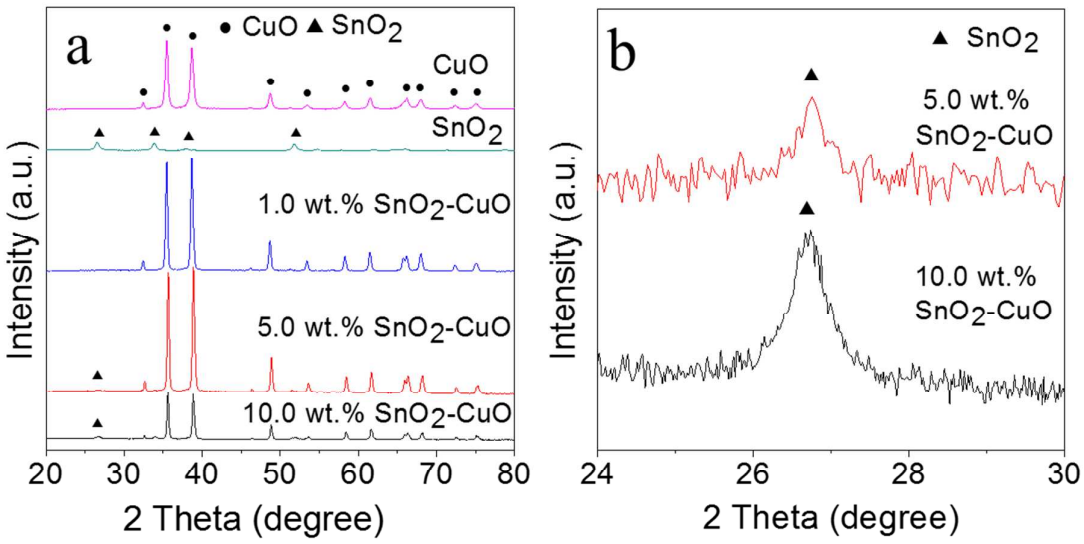

Fig. 3 XRD patterns of CuO NRs, SnO_2 NPs, 1.0 wt.% SnO_2-CuO, 5.0 wt.% SnO_2-CuO, and 10.0 wt.% SnO_2-CuO (a), enlarged view in the 2θ range of 24-30° of 5.0 wt.% SnO_2-CuO and 10.0 wt.% SnO_2-CuO (b).

Table 1 The physical parameters of all the samples.

Sample	d_{CuO}[a] (nm)	d_{SnO2}[a] (nm)	T_{TPR}[b] (^oC)	T_M[c] (^oC)	S_{BET}[d] ($m^2 g^{-1}$)
CuO	28.4	-	180-280	242	17.2
SnO_2	-	21.9	450-690	604	29.4
1.0 wt.% SnO_2-CuO	30.7	-	180-350	281	5.5
5.0 wt.% SnO_2-CuO	30.4	20.1	150-370	274	7.4
10.0 wt.% SnO_2-CuO	31.2	21.5	165-380	256	8.6
1.0 wt.% SnO_2+CuO	28.4	21.9	180-490	324	2.5

[a] The crystal size of CuO and SnO_2 calculated from the XRD patterns.

[b] Reduction temperature range of the samples.

[c] Temperatures at the peak maximum.

[d] The BET surface area of the samples.

Fig. 4 shows the TEM images of the prepared samples, which are all highly crystallized. As shown in Fig. 4a, the as-prepared CuO sample has rod morphology with a diameter of 200-400 nm, in agreement with the above SEM results (Fig. 2b). Figure. 4b indicates that the as-obtained SnO_2 exhibits an almost spherical shape with an average size of about 25 nm. In the case of SnO_2-CuO hybrid, a large number of SnO_2 NPs can be seen deposited on the surface of CuO NRs uniformly, forming mace-like structure (Fig. 4c and Fig. S4, S5 in Supporting Information). Representative magnified high-resolution transmission electron microscope (HRTEM) images as shown in Fig. 4d and 4e reveal that the SnO_2-CuO hybrid sample has a high crystallinity, possessing clear lattice spacing of about 0.25 nm and 0.33 nm, which correspond to (-111) and (110) planes of CuO and SnO_2, respectively. Also, the interfacial regions between CuO and SnO_2 indicated by white lines are

clearly observed.

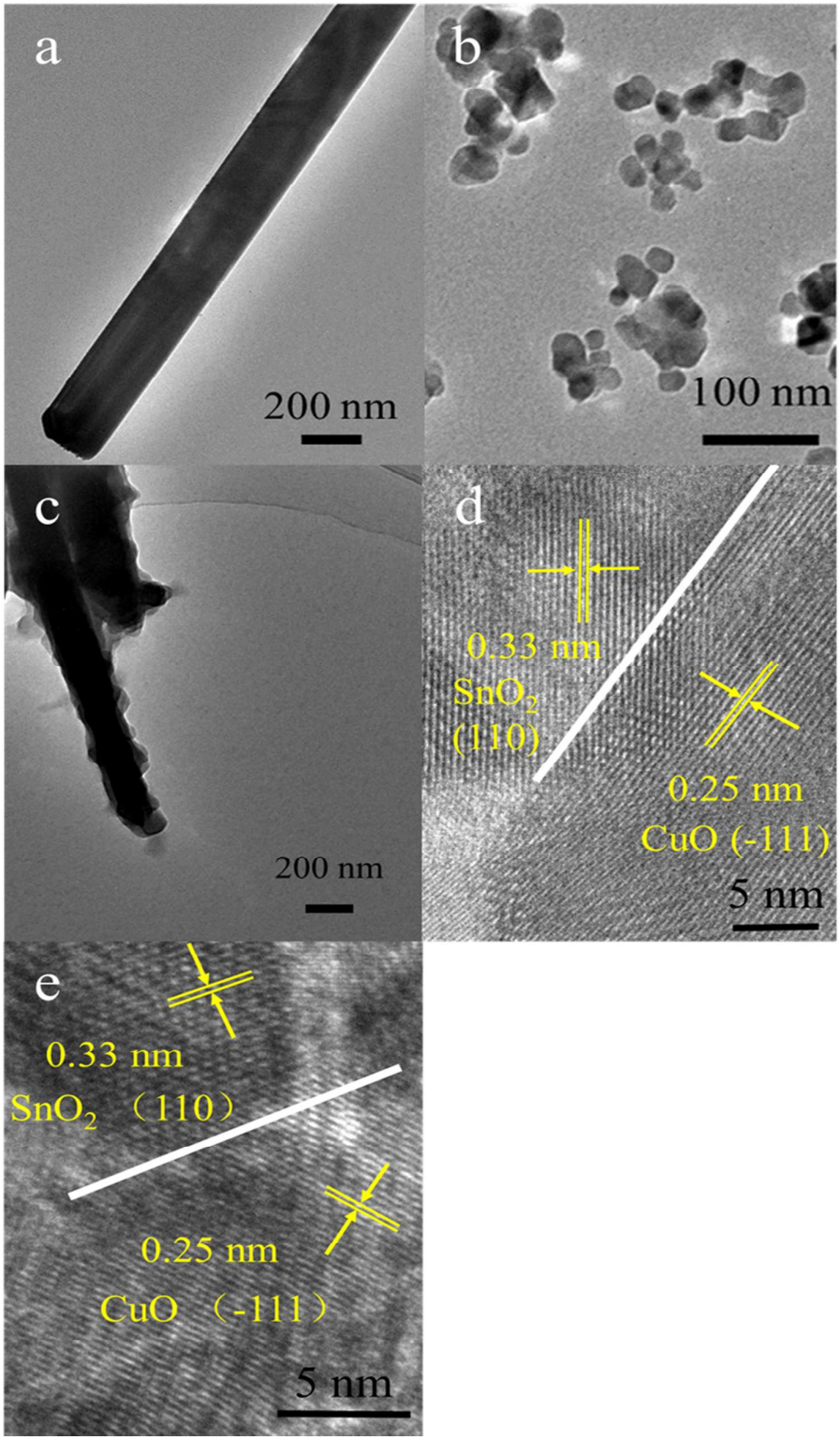

Fig. 4 TEM images of CuO NRs (a), SnO_2 NPs (b) and 1.0 wt.% SnO_2-CuO (c), and HRTEM images of 1.0 wt.% SnO_2-CuO (d, e).

A further characterization of the structure of the typical 1.0 wt.% SnO_2-CuO hybrid was carried out by high angular annular dark field scanning transmission electron microscopy (HAADF-STEM) (Fig. 5a, b), which displays obvious hybrid mace-like nanostructures, consistent with the above SEM and HRTEM observations. The EDS mapping results in Fig. 5(c-f) demonstrates the actual distributions of Cu, Sn, and O elements separately in the single SnO_2-CuO hybrid. Clearly, all of them are evenly dispersed, matching well with the results of the above SEM characterizations (Fig. 2f-h). In short, these characterizations support the successful synthesis of the SnO_2-CuO mace-like nanostructure with SnO_2 NPs loaded on the CuO NRs uniformly using our strategy.

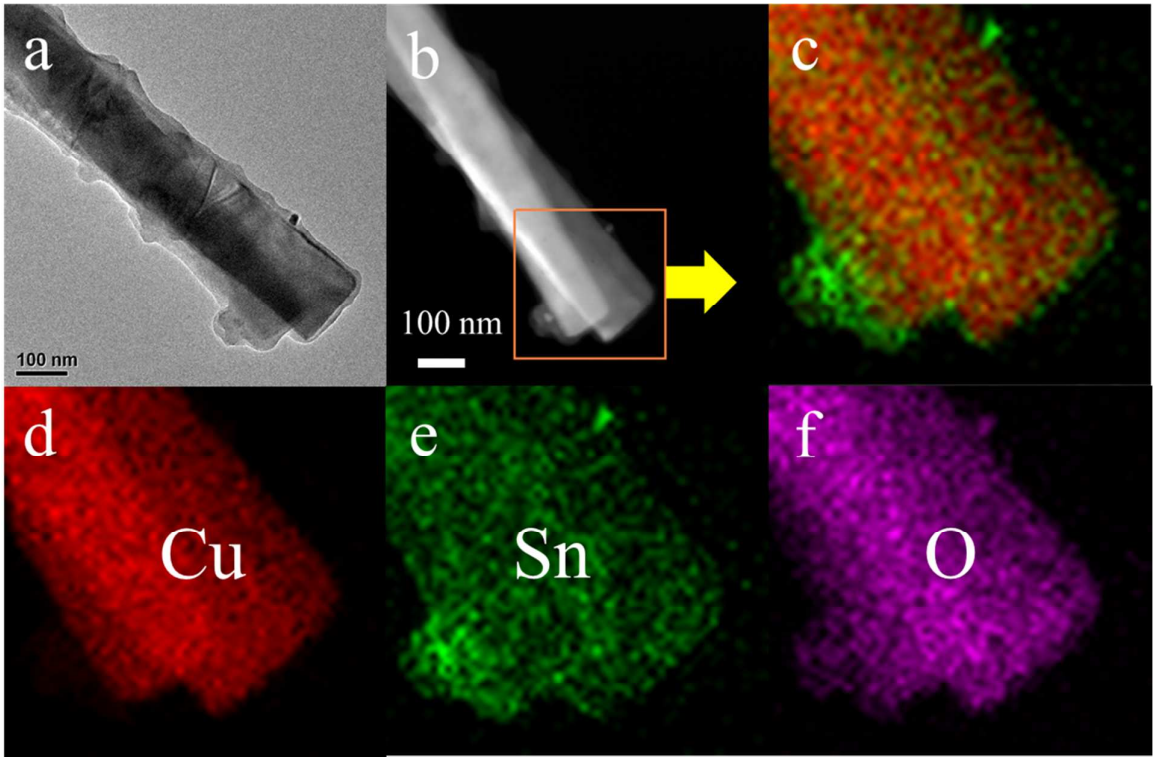

Fig. 5 TEM image (a), HAADF-STEM image (b), and combined mapping image (c) of 1.0 wt.% SnO_2-CuO, elemental mapping images of Cu (d), Sn (e), and O (f).

It should be pointed out that the presence of PVP is crucial for the successful preparation of the SnO_2-CuO hybrids. In a control experiment without using PVP, plentiful pre-made SnO_2 NPs were

directly added to the CuO NRs suspension in ethanol and the mixture was further stirred for 24 h. TEM images of the resulting product (Fig. S6 in Supporting Information) show that most of the SnO_2 NPs are not deposited on the surface of the CuO NRs and become severely agglomerated, indicating that PVP attached on the CuO NRs provides a strong anchor on the surface for the SnO_2 species.

3.2. Catalytic property

Table 2 shows the catalytic performance of all the samples for M2 synthesis via the Rochow reaction at 295 ^{o}C under atmospheric pressure for 24 h. As displayed, the SnO_2 NPs appeares to be inactive. In contrast, the pure CuO NRs give a low M2 selectivity of 40.1% and Si conversion of 12.5% under the same reaction conditions. The catalytic performance for physically mixed CuO NRs and SnO_2 NPs is not improved, in which the Si conversion and M2 selectivity should be contributed by the CuO NRs. Interesingly, the 1.0 wt.% SnO_2-CuO hybrid nanocatalysts gives a drastically enhanced M2 selectivity (78.9%) and Si conversion (56.3%) under identical conditions. We have previously reported that the catalytic activities of CuO catalysts can be increased upon forming composites with ZnO, which is attributed to the synergetic effects of CuO with ZnO.[22] Similarly, the enhanced activity of the hybrids in this work should be caused by the synergistic interaction between CuO and SnO_2. However, the catalyst performance becomes poorer dramatically again with the further increase of SnO_2/CuO ratio, possibly due to the excess SnO_2 would block the active sites of CuO. It is also found that the catalyst performances decreases when the SnO_2/CuO ratios are less than 1%, indicating that the optimized ratio is 1.0 wt.%. Furthermore, the catalytic property of the 1 wt.% SnO_2-CuO hybrid is compared with that of previous reported (see Table S1). Although the test condition such as catalyst amount and reaction temperature is

different among these catalysts, it is found that our catalyst, 1 wt.% SnO_2-CuO, exhibited excellent M2 selectivity (90.1%) and yield (45.5%) even using much lower amount. It should be pointed out here that the error bars for both conversion and selectivity are ±0.1% and all the catalytic data obtained by at least three repeated experiments using the same silicon. These results demonstrate that the prepared catalysts possessing nanoscale heterostructures with proper CuO and SnO_2 ratio have the best catalytic performance. In addition, byproducts such as M1, M3, M1H, M2H, LB, and HB with a negligible difference over the various prepared catalysts are also detected except for SnO_2 sample.

Table 2 Catalytic performance of all the catalysts for Rochow reaction.

Sample	Product selectivity (%)							C-Si (%)
	M1	M2	M3	M1H	M2H	LBR	HBR	
CuO	26.3	40.1	1.8	2.6	4.7	12.9	22.6	12.5
SnO_2	-	-	-	-	-	-	100	3.1
0.1 wt.% SnO_2-CuO	18.5	70.9	1.9	0.4	2.9	2.0	3.4	18.9
0.2 wt.% SnO_2-CuO	17.2	76.5	0.7	0.2	1.6	1.1	2.7	22.3
0.5 wt.% SnO_2-CuO	11.9	78.1	1.4	0.2	1.9	1.7	4.8	32.1
1.0 wt.% SnO_2-CuO	11.2	78.9	1.2	0.6	2.3	1.6	4.2	56.3
5.0 wt.% SnO_2-CuO	13.3	25.4	1.6	0.6	2.9	3.5	52.7	10.2
10.0 wt.% SnO_2-CuO	15.4	5.6	2.7	0.3	1.1	4.6	70.3	7.9
1.0 wt.% SnO_2+CuO	16.2	21.3	1.7	5.2	2.7	16.9	36.0	5.9

Fig. 6a shows the XRD patterns of the waste contact masses (catalysts mixed with silicon after reaction at 295 ^{o}C). It can be seen that the waste contact masses are composed of Si and Cu, but

lack of CuO and Cu_2O species. The formation of Cu may originate from the reaction of MeCl with the lattice oxygen of the Cu-based catalysts.[24] An enlarged view of the XRD patterns in the range of 40-75° (Fig. 6b) for CuO, 1.0 wt.% SnO_2-CuO hybrid and 1.0 wt.% SnO_2+CuO hybrid show the presence of Cu_3Si species, suggesting the formation of alloyed Cu_xSi active intermediate during the reaction. In the Rochow reaction, Cu_3Si is normally regarded as the key catalytic active specie,[25] through which, MCSs are produced. When Cu and Si are brought together at elevated temperatures in the presence of MeCl gas, Cu_3Si will be formed.[26] The amount of Cu_3Si can substantially affect the M2 selectivity and Si conversion.[11] As noticed, the intensity of Cu_3Si peaks for 1.0 wt.% SnO_2-CuO is much higher than that of the others, suggesting that 1.0 wt.% SnO_2-CuO hybrid is more active in generating Cu_xSi than the others. This may be due to the proper proportion of SnO_2 and CuO creates a stronger synergistic effect and more intimate contacts between the catalyst and the solid Si, thus promoting the formation of active Cu_3Si phases, which is the key contribution to enhance the catalytic activity for M2 production.

To further study the synergetic effect of CuO and SnO_2, the catalysts were investigated by H_2-TPR. Fig. 6c shows the H_2-TPR curves of all the samples. The peak temperatures (T_M) and reduction temperature range of the samples are compiled in Table 1. As shown, for the pure CuO and SnO_2 samples, the reduction peaks are clearly observed in the range of 180-280 ^oC and 450-690 ^oC, respectively. However, in the case of the 1.0 wt.% SnO_2-CuO sample, there appear two reduction peaks and the peak position shifts to the lower temperature range as compared with those of the sole CuO and SnO_2, respectively. The above shifts should be attributed to synergistic interaction between CuO and SnO_2.[27-29]

We further carried out the XPS analysis to elucidate the interaction between the two components.[18] As shown in Fig. 6d, the characteristic intense peaks at 934.3 and 953.7 eV are

assigned to Cu2p3/2 and Cu2p1/2 of CuO NRs with binding energy calibrated with C1s = 284.8 eV.[30] The peak around 943.8 eV is attributed to the shakeup line of CuO.[10] However, the binding energy of Cu2p3/2 and Cu2p1/2 in the SnO_2-CuO hybrids are decreased by 0.35 and 0.33 eV respectively as compared with that of CuO NRs, and the shakeup line at 943.8 eV is almost disappeared, implying the change in the chemical state of Cu.[31] In addition, for SnO_2 NPs, the binding energies of Sn 3d5/2 and Sn 3d3/2 are located at 495.4 and 487.0 eV, respectively, which are similar to those for SnO_2 (Fig. 6e).[32] But in the case of 1.0 wt.% SnO_2-CuO hybrid, the observation of the higher, weaker and broader peaks compared to those of the single SnO_2 indicates the electron-deficient state of Sn.[33] Hence, the above observed peak shifts should be attributed to electron transfer from SnO_2 to CuO,[34] which leads to strong synergistic interaction in the SnO_2-CuO hybrid, thus enhancing the catalytic activities for the Rochow reaction. In addition, the O 1s peak was located at 529.8 eV and 530.8 eV for the CuO and SnO_2, respectively, as shown in Fig. 6f, suggesting that the oxidation state of O is - 2 in CuO[35] and SnO_2 sample.[36]

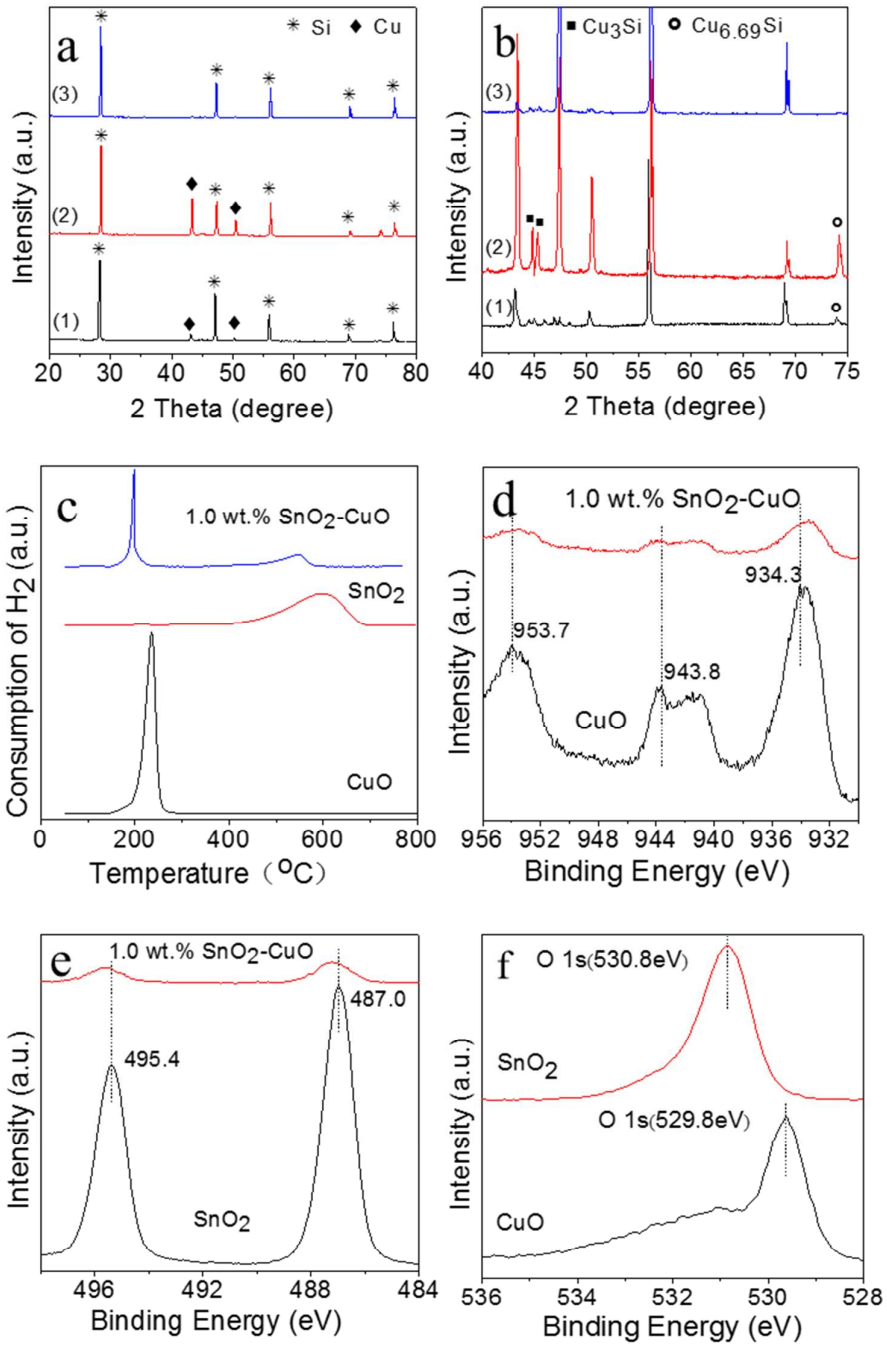

Fig. 6 XRD patterns of waste contact masses (CuO (1), 1.0 wt.% SnO_2-CuO (2), 1.0 wt.% SnO_2+CuO (3) mixed with silicon after reaction at 295 ^oC) (a), enlarged view in the 2θ range of 40-75° (b) of CuO (1), 1.0 wt.% SnO_2-CuO (2), 1.0 wt.% SnO_2+CuO (3), H_2-TPR curves of the CuO, SnO_2 and 1.0 wt.% SnO_2-CuO samples (c), Cu 2p spectrum of CuO and 1.0 wt.% SnO_2-CuO samples (d), Sn 3d spectrum of SnO_2 and 1.0 wt.% SnO_2-CuO samples (e), O 1s spectrum of CuO and SnO_2 samples (f).

The SEM image of the contact masses before the reaction (Fig. 7a) shows that the Si surface is smooth, and densely and uniformly distributed with catalyst particles (insert of Fig.7a). However，after the reaction, the Si surface became coarse or porous (Fig. 7b), suggesting the occurrence of etching process during the reaction, consistent with the so-called anisotropic etching reaction mechanis,[37] and indicating that the 1.0 wt.% SnO_2-CuO catalyst is very active for the Rochow reaction. The element mapping images show the distribution of the elements Si (Fig. 7c) and Cu (Fig. 7d) on the surface of the waste contact mass. As displayed, the Si mapping image clearly shows the presence of the reacted (dark red) and unreacted (bright red) zones of Si particle, while Cu (bright green) is distributed uniformly on the reacted or etched Si surface, indicating the occurrence of catalytic reaction between Si particles and Cu-based catalysts. Therefore, based on the above results, we can schematically illustrate the Rochow reaction process as displayed in Fig. 7e. In the process, a large quantity of Si is fully mixed with a small quantity of the SnO_2-CuO hybrid before the reaction. With diffusion of SnO_2-CuO hybrid into the Si matrix, the Cu_xSi alloy is gradually formed at the interface between SnO_2-CuO catalyst and the Si at the elevated temperatures. In the reaction the bulk solid phase presented at reacting surface regions of Si particles is Cu_xSi, which reacts with the gas MeCl to form MCSs. As the reaction proceeds, metallic copper is continuously produced with the reduction of Cu_xSi alloy until the catalyst is deactivated.

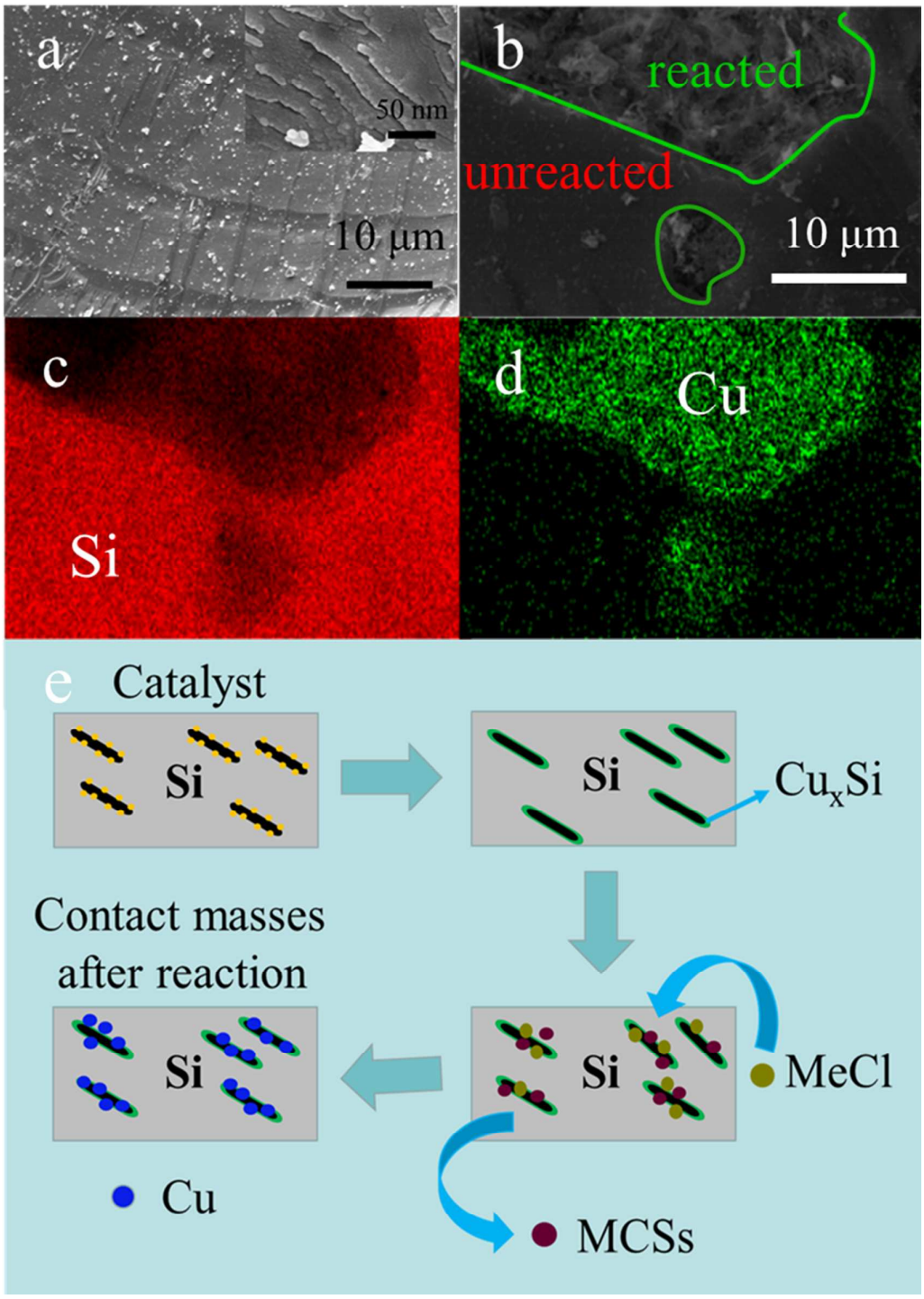

Fig. 7 SEM images of contact masses before (a) and after (b) reaction, elemental mapping images of Si (c), Cu (d), and schematic illustration of the Rochow reaction process (e).

4. Conclusions

In summary, SnO_2-CuO hybrid mace-like nanocatalysts are prepared by simply depositing pre-made SnO_2 NPs on CuO NRs in the presence of PVP. It is observed that SnO_2 NPs are distributed on CuO NRs evenly generating a lot of heterojunctions. This process is facilitated by PVP molecules. When applied to the Rochow reaction, the SnO_2-CuO hybrid nanocatalysts exhibit superior catalytic activities to CuO NRs, SnO_2 NPs and their mixture. This activity enhancement is attributed to the enhanced synergistic interaction between CuO and SnO_2 in the designed nanocatalysts, as evidenced by the shifts of Cu2p and Sn3d in the XPS spectra, together with the shifts of reduction peaks of CuO and SnO_2 in the TPR profiles. This work provides conducive clues to design efficient nanoscale hetero-structured catalysts for Rochow reaction.

Acknowledgements

The authors gratefully acknowledge the financial supports from the National Natural Science Foundation of China (no. 51272252 and 21206172). Z. Z is grateful to the kind supports of both Nanyang Technological University (NTU) and Institute of Chemical Engineering and Sciences (ICES) under Agency for Science, Technology and Research (A*STAR).

Appendix A. Supplementary material

Supplementary data associated with this article can be found, in the online version, at…

References

1 J. M. Bablin, L. N. Lewis, P. Bui and M. Gardner, *Ind. Eng. Chem.Res.*, 2003, **42**, 3532-3543.

2 R. J. H. Voorhoeve, J. A. Lips and J. C. Vlugter, *J. Catal.*, 1964, **3**, 414-425.

3 H. Ehrich, D. Born, K. Richter, J. RichterMendau and H. Lieske, *Appl. Organomet. Chem.*, 1997, **11**, 237-247.

4 H. Lieske and R. Zimmermann, *Catal. Lett.*, 1995, **33**, 413-420.

5 A. D. Gordon, B. J. Hinch and D. R. Strongin, *Catal. Lett.*, 2009, **133**, 14-22.

6 E. G. Rochow, *J. Am. Chem. Soc.*, 1945, **67**, 963-965.

7 Z. Patense, Marken and Z. Li, *DTP-2212218*, 1973.

8 W. Kalchauer, H. Straussberger, W. streckel and J. Gross, *USP-6211394*, 2001.

9 L. Zhang, S. Hao, C. H. Yang, J. Li, K. Yang, C. F. Hu and S. B. Ge, *Appl. Organomet. Chem.*, 2011, 25, 508-513.

10 Z. L. Zhang, H. W. Che, Y. L. Wang, J. J. Gao, L. R. Zhao, X. L. She, J. Sun, P. Gunawan, Z. Y. Zhong and F. B. Su, *Ind. Eng. Chem. Res.*, 2012, **51**, 1264-1274.

11 L. N. Lewis and W. J. Ward, *Ind. Eng. Chem. Res.*, 2002, **41**, 397-402.

12 N. Siegfried, Burghausen and B. Upper, *USP-2666776*, 1954.

13 D. H. Hashiguchi, R. J. Dietrich and G. P. Schoepe, *USP-4503165*, 1985.

14 A. D. Gordon, B. J. Hinch and D. R. Strongin, *J. Catal.*, 2009, **266**, 291-298.

15 Z. L. Zhang, H. W. Che, Y. L. Wang, X. L. She, J. Sun, P. Gunawan, Z. Y. Zhong and F. B. Su, *ACS Appl. Mater. Interfaces*, 2012, **4**, 1295-1302.

16 Z. L. Zhang, H. W. Che, Y. L. Wang, J. J. Gao, X. L. She, J. Sun, Z. Y. Zhong and F. B. Su, *RSC Adv.*, 2012, **2**, 2254-2256.

17 Z. L. Zhang, H. W. Che, Y. L. Wang, L. Y. Song, Z. Y. Zhong and F. B. Su, *Catal. Sci. Technol.*,

2012, **2**, 1953-1960.

18 Z. L. Zhang, H. W. Che, Y. L. Wang, J. J. Gao, Y. Ping, Z. Y. Zhong and F. B. Su, *Chem. Eng.J.*, 2012, **211**, 421-431.

19 H. P. Martin, G. Irmer and E. Muller, *J. Eur. Ceram.Soc.*, 1998, **18**, 193-199.

20 G. Avgouropoulos, T. Ioannides and H. Matralis, *Appl. Catal. B: Environ.*, 2005, **56**, 87-93.

21 L. Li, D. S. Mao, J. Yu and X. M. Guo, *Appl. Catal. B: Environ.*, 2015, **279**, 394-404.

22 Y. X. Zhu, Y. L. Wang, L. Y. Song, X. Chen, W. Y. Liu, J. Sun, X. L. She, Z. Y. Zhong and F. B. Su, *RSC Adv.*, 2013, **3**, 9794-9802.

23 Q. Qi, P. P. Wang, J. Zhao, L. L. Feng, L. J. Zhou, R. F. Xuan, Y. P. Liu and G. D. Li, *Sensors and Actuators B*, 2014, **194**, 440-446.

24 L. N. Lewis, W. V. Ligon and J. C. Carnahan, *Silicon Chem*, 2002, **1**, 23-25.

25 L. Levin, Z. Atzmon, A. Katsman and T. Werber, *Mater. Chem. Phys.*, 1995, **40**, 56-61.

26 L. Stolt and F. M. Dheurle, *Thin Solid Films*, 1990, **189**, 269-274.

27 M. F. Luo, Y. J. Zhong, X. X. Yuan and X. M. Zheng, *Appl. Catal. A*, 1997, **162**, 121-131.

28 M. F. Luo, J. M. Ma, J. Q. Lu, Y. P. Song and Y. J. Wang, *J. Catal.*, 2007, **246**, 52-59.

29 R. Lin, M. F. Luo, Y. L. Xie, Y. J. Zhong and W. P. Liu, *React. Kinect. Catal. Lett.*, 2004, **81**, 65-71.

30 S. Velu, K. Suzuki, Chinnakonda S. Gopinath, H. Yoshida and T. Hattoric, *Phys. Chem. Chem. Phys.* 2002, **4**, 1990-1999.

31 J. Kim, W. Kim and K. Yong, *J. Phys. Chem. C*, 2012, **116**, 15682-15691.

32 G. Samjeske, S. I. Nagamatsu, S. Takao, K. Nagasawa, Y. Imaizumi, O. Sekizawa, T. Yamamoto, Y. Uemura, T. Urugaad and Y. Iwasawa, *Phys. Chem. Chem. Phys.* 2013, **15**, 17208-17218.

33 M. E. Yu, C. T. Li, G. M. Zeng, Y. Zhou, X. N. Zhang and Y. E. Xie, *Appl. Surf. Sci.*, **2015**, 342, 174-182.

34 K. I. Choi, H. J. Kim, Y. C. Kang and J. H. Lee, *Sensors and Actuators B*, 2014, **194**, 371-376.

35 U. Arellano, J. M. Shen, J. A. Wang, M. T. Timko, L. F. Chen, J. T. V. Rodriguez, M. Asomoza, A. Estrella, O. A. G. Vargas and M. E. Llanos, *Fuel*, 2015, **149**, 15-25.

36 J. Ding, Z. Li, H. L. Wang, K. Cui, A. Kohandehghan, X. H. Tan, D. Karpuzovc and D. Mitlin, *J. Mater. Chem. A*, **2015**, 3, 7100-7106.

37 Z. Y. Liu, H. W. Bai, S. P. Xu and D. D. Sun, *Int. J. Hydrogen Energy*, 2011, **36**, 13473-13480.